ACCOUNTS
—of materials research—

pubs.acs.org/amrcda Article

Intense Pulsed Light-Driven Flash Thermal-Shock Synthesis: A Frontier Strategy for Ultrafast Nanomaterial Design

Euichul Shin,[#] Dogyeong Jeon,[#] Hamin Shin, Jun-Hwe Cha, and Il-Doo Kim*

Cite This: https://doi.org/10.1021/accountsmr.6c00058 Read Online

ACCESS | Metrics & More | Article Recommendations

CONSPECTUS: Ultrafast annealing represents a paradigm shift in materials synthesis, compressing thermal processing into millisecond-to-subsecond time scales. This approach establishes a unique kinetic-control regime that can enable metastable phases, defect-rich surfaces, engineered interfaces, and atomic-level catalyst functionalization while suppressing thermal degradation that often accompanies conventional furnace-based treatments under equilibrium conditions. Resistive Joule-heating approaches (e.g., carbothermal shock) require conductive supports, whereas laser-based methods often face limitations in uniformity and large-area scalability. Among various ultrafast techniques, light-based approaches offer significant advantages in terms of material compatibility, enabling a broad range of applications. In particular, intense pulsed light (IPL)-driven flash thermal-shock synthesis (FTS) is especially attractive because, unlike general photothermal annealing that typically relies on more moderate optical heating, FTS uses high-intensity broadband xenon-flash pulses to induce a thermal shock within milliseconds. Operating via rapid photothermal conversion, FTS instantaneously achieves ultrahigh temperatures (>2000 K) and rapid heating and cooling rates (10^4–10^6 K s^{-1}). Over the past decade, this flash-processing concept has evolved into a versatile nanomaterials platform capable of converting precursors into functional, often metastable materials under strongly nonequilibrium conditions.

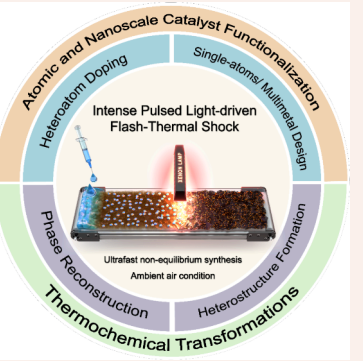

In this Account, we first introduce the fundamental photothermal mechanisms and time−temperature characteristics governing FTS. We outline key considerations for material selection—focusing on the strong light-absorption capabilities of carbonaceous materials, defect-engineered metal oxides, and plasmonic metals—alongside the critical metrological challenges of millisecond-scale transient temperature measurement via high-speed infrared pyrometry. We then survey representative nanoengineering strategies enabled by FTS across four major categories. First, atomic-level engineering emphasizes low-thermal-budget heteroatom incorporation (e.g., rapid boron doping into graphene without combustion in ambient air) and the robust stabilization of high-density single-atom catalysts. The ultrafast quenching effectively traps isolated metal atoms at defect sites before diffusion-driven clustering can occur. Second, nanoparticle functionalization covers the transition from monometallic decoration to complex multimetallic and high-entropy alloy (HEA) systems. By leveraging high temperatures to overcome conventional miscibility barriers and rapidly freezing the resulting highly distorted atomic configurations, FTS produces uniformly dispersed HEAs and core(HEA)@shell heterostructures. Third, surface and defect engineering highlight the FTS ability to activate nanomaterial surfaces through rapid reduction, oxygen-vacancy generation, and local modulation of the coordination environment, thereby creating catalytically and electronically active states. Fourth, thermochemical transformations induced by ultrafast photothermal pulses include porosity generation, phase reconstruction, carbothermic synthesis, and heterostructure formation. This also includes transforming nanodiamonds into carbon nanoonions and synthesizing metastable transition metal carbides via carbothermic reactions. Finally, we outline the remaining challenges and future opportunities critical for advancing this field. To guide the rational design of nanomaterials via FTS, we highlight the necessity of expanding the accessible compositional space, developing absorber engineering for nonphotothermal substrates, implementing precise atmosphere programming, and deploying millisecond-resolved in situ and operando analyses to deepen fundamental mechanistic understanding.

1. INTRODUCTION

Thermal energy plays a central role in supplying the activation energy required for a broad range of chemical and structural processes.[1] In particular, the key chemical reactions in chemiresistive gas sensors and heterogeneous catalysts predominantly occur at surfaces, making surface engineering essential for achieving high performance.[2,3] However, conventional annealing typically relies on slow thermal radiation,

Received: March 5, 2026
Revised: April 15, 2026
Accepted: May 5, 2026

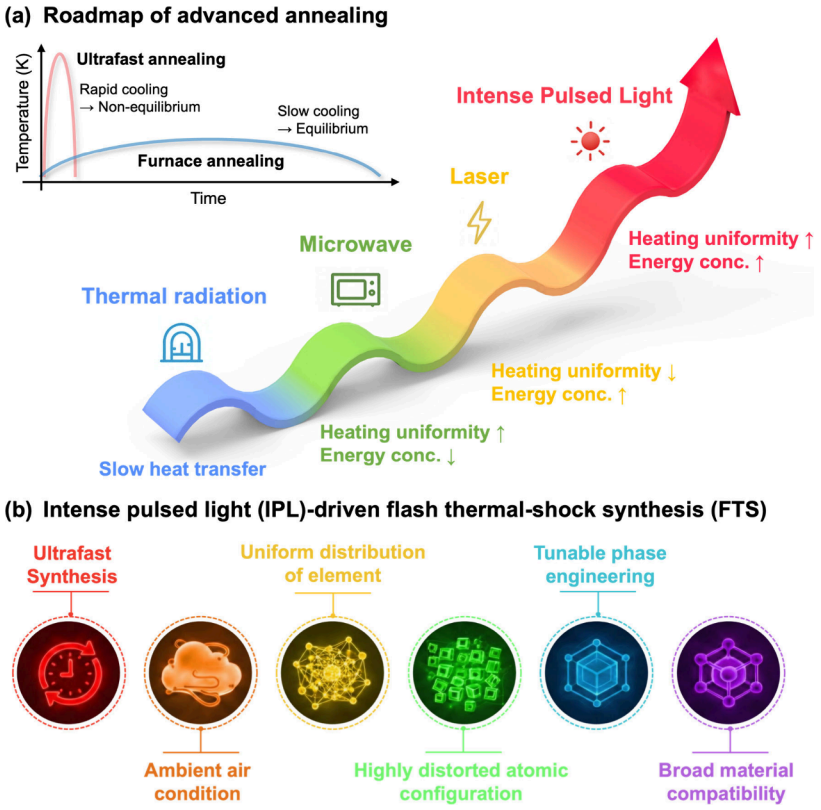

Figure 1. (a) Roadmap of advanced annealing. (b) Advantages of intense pulsed light (IPL)-driven flash thermal-shock synthesis (FTS).

Table 1. Comparative Analysis of Ultrafast Annealing Strategies for Nanomaterial Design

Feature	Continuous-wave laser	Nonresistive (microwave/plasma)	Resistive (Joule/induction)	IPL-driven FTS
Operating temperature	High	Plasma: >8000 K	Extremely high (>2000 K)	Extremely high (2000−3000 K)
Heating/cooling rate	Extremely high	Moderate to high	High	Extremely high (10^6 K s^{-1})
Material compatibility	Selective absorption	Depends on dielectric/ionized gas	Conductive substrates	Universal (oxides, carbons, and more)
Scalability	Point-by-point scanning	Limited by nonuniformity/instability	High	High (large-area broadband emission)
Energy efficiency	Moderate	Varies (often weak)	High	High
Controllability	Spatial scanning control	Field/plasma stability issues	Voltage/current control	Temporal pulse, atmosphere control

leading to bulk heat transfer rather than surface-selective activation. This equilibrium-based approach often leads to particle aggregation or sintering, resulting in a loss of active surface area and limiting precise control over nanoscale structures.

To overcome these thermodynamic limitations and minimize thermal budgets, various annealing strategies have evolved, as illustrated in the roadmap of advanced annealing (Figure 1a). Ultrafast annealing has emerged as a versatile kinetic-control approach for advanced nanomaterial design.[4] Depending on the heating mechanism, ultrafast annealing can be categorized into resistive and nonresistive modes. Resistive heating, such as direct Joule or induction heating, requires electrically conductive substrates to generate heat through current flow.[5,6] In contrast, nonresistive techniques, including microwave and plasma heating, utilize electromagnetic fields or ionized gases. Although plasma heating can achieve extremely high temperatures (>8000 K), it suffers from instability and limited scalability.[7] Microwaves, in contrast, deliver relatively weak and nonuniform energy.[8]

In this regard, light-driven ultrafast heating has emerged as a highly controllable and stable alternative, offering both spatially uniform irradiation and exceptionally high heating rates. Light-based ultrafast annealing is typically implemented using monochromatic continuous-wave laser annealing or broadband intense pulsed light (IPL) irradiation.[9−11] Among them, IPL-driven flash thermal-shock synthesis (FTS) utilizes broadband light to generate strong photothermal effects, rapidly elevating the surface temperature to 2000−3000 K within milliseconds with a rapid ramping rate (up to ~10^6 K s^{-1}).[12] FTS differs from resistive methods in compatibility with a wider range of materials, including oxides and semiconductors. The broadband xenon emission further enables cost-effective, energy-efficient, large-area processing compared with laser annealing (Table 1). As highlighted in Figure 1b, FTS creates a unique kinetic-control regime that offers distinct advantages over conventional methods, characterized by six key features. The FTS enables millisecond-scale high-temperature processing with ultrafast quenching, enabling ambient-air reactions while suppressing aggregation and enabling phase/defect engineering across carbon, oxide, and chalcogenide systems. Together, these features make FTS a powerful platform for the design of kinetic materials beyond conventional thermodynamic limits.

In this Account, we explore versatile strategies for nanoengineering through light-driven ultrafast heating, with a particular focus on FTS. We begin by introducing the

https://doi.org/10.1021/accountsmr.6c00058
Acc. Mater. Res. XXXX, XXX, XXX−XXX

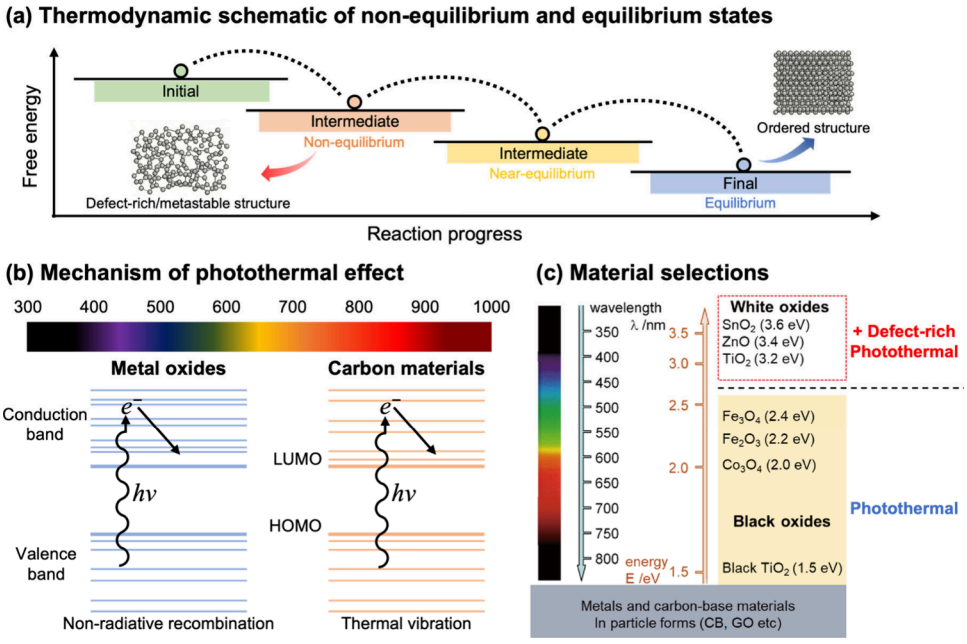

Figure 2. Principles of FTS. (a) Schematic energy landscape showing how pulsed heating enables access to intermediate nonequilibrium states prior to relaxation toward near-equilibrium phases. (b) Schematic illustrations of mechanism of photothermal effect. Reproduced with permission from ref 48. Copyright 2019 Royal Society of Chemistry. (c) Representative classes of materials that are suitable for FTS, according to their optical band gaps and electronic structures. Reproduced with permission from ref 26. Copyright 2025 American Chemical Society.

fundamental mechanisms underlying IPL-induced photothermal effects that drive ultrafast annealing. The discussion spans photothermal engineering across four themes: (1) Atomic-Level Engineering (heteroatom doping and single atom catalysts), (2) Nanoparticle Functionalization (mono- to multielemental systems), (3) Porosity Generation and Phase Reconstruction, and (4) Heterostructure Formation. Finally, we summarize light-driven ultrafast annealing methods, highlight remaining challenges, and offer perspectives that provide deep insights into the potential of IPL-based kinetic materials design.

2. PRINCIPLES OF FLASH THERMAL-SHOCK SYNTHESIS

2.1. Mechanism of Flash Thermal-Shock Synthesis

Intense pulsed light (IPL)-driven flash thermal-shock synthesis (FTS) is highly attractive because it delivers broadband xenon emission spanning UV to near-IR across large areas without direct contact. By using millisecond-duration pulses, this method enables rapid, spatially programmable heat delivery. FTS represents a paradigm shift in materials processing, diverging fundamentally from conventional equilibrium-based methods (Figure 2a). Conventional furnace sintering typically follows a slow ramping and cooling profile, maintaining the material at thermodynamic equilibrium or near-equilibrium states for extended periods. In contrast, FTS is characterized by an ultrafast heating rate (10^4–10^6 K s^{-1}), a millisecond-scale duration (<20 ms), and a rapid cooling rate.[13] This temporal compression allows the system to reach extremely high temperatures (>2000 K) instantaneously, accessing a kinetic regime that is practically unreachable by steady-state heating methods. Upon flash heating, the system is rapidly driven far from equilibrium, resulting in an intermediate, nonequilibrium state. In this regime, extremely high temperatures are applied over such short durations that the system is precluded from fully relaxing to its equilibrium state. This process facilitates the formation of metastable phases, ultrafine nanostructures, and highly defective surfaces, which are typically inaccessible via conventional slow-heating techniques.[14]

The driving force behind FTS is the photothermal effect, where incident photons are absorbed by a material and converted into thermal energy. The mechanism depends heavily on the electronic structure, as depicted in Figure 2b. When a material absorbs photons over a broad wavelength range, the incident light excites electrons from lower-energy states to higher-energy states. In metallic nanostructures, localized surface plasmon resonance occurs when the wavelength of incident light matches that of the conduction-band electrons.[15] The nonradiative decay of this collective oscillation via Landau damping generates hot carriers that promote nanowire growth or nanoparticle (NP) sintering at reduced temperatures before transferring thermal energy to the lattice through electron–electron and electron–phonon scattering.[16] For semiconducting oxides and chalcogenides, photons with energy exceeding the bandgap ($h\nu > E_g$) excite electrons from the valence band to the conduction band.[15] The relaxation of these excited carriers occurs predominantly via nonradiative recombination, releasing energy as phonons. Carbon-based materials are widely employed as photothermal media due to their strong light absorption and efficient electron–phonon coupling. Conductive carbon materials such as carbon nanofibers (CNFs), carbon black (CB), and graphene exhibit broadband absorption arising from their conjugated carbon domains.[17] In these systems, photoexcitation is followed by nonradiative relaxation, leading to efficient conversion of photon energy into lattice vibrations. In contrast, graphene oxide (GO) possesses an insulating to wide-bandgap semiconducting behavior, compared to pristine graphene's zero-bandgap semimetal character.[18] Under light irradiation, localized sp^2 domains and defect-/oxygen-related electronic

https://doi.org/10.1021/accountsmr.6c00058
Acc. Mater. Res. XXXX, XXX, XXX−XXX

states in absorb photons and promote electrons from occupied to unoccupied states.[19] The subsequent nonradiative relaxation efficiently transfers energy to the lattice, inducing intense molecular and lattice vibrations. Under intense irradiation, these photothermal effects partially reduce GO (rGO), restore larger sp^2 domains, and thereby enhance its photothermal response.[20,21] By tailoring the density of electronic states, defect levels, and coupling between electrons and phonons, one can enhance this photon-to-heat conversion efficiency.[22]

The time scale of light-material interactions governs the thermodynamic and kinetic behaviors during FTS. Upon light irradiation, a sequence of processes, including photon absorption, photothermal conversion, lattice thermalization, and subsequent heat dissipation, unfolds over time scales ranging from femtoseconds to milliseconds.[23] To exploit this spatially confined thermal energy, the system is designed with two distinct components: a light-absorbing "host" that acts as a heat source, and adjacent "reactive guest" species that undergo chemical transformation. The utility of FTS lies in its ability to manipulate the thermodynamic and kinetic landscape of material formation through the efficient thermal transfer between these components. During the heating stage, photothermal absorption by the host rapidly raises its lattice temperature, which is then conducted to the guest precursors. This intense thermal trigger drives the guest species far above their decomposition and diffusion thresholds, initiating rapid pyrolysis, reduction, or carbothermal reactions and enabling the nucleation of new phases under nonequilibrium conditions.[24,12] Because the pulse duration of FTS is extremely short, long-range atomic diffusion and coarsening are kinetically suppressed, while local rearrangements such as exsolution of metal species, and formation of short-range ordered or amorphous domains are promoted, often yielding single atoms, ultrafine NPs, or heterostructured interfaces directly on the support.[20,25−27]

2.2. Material Selection and Engineering for Flash Thermal-Shock Synthesis

The feasibility of FTS depends on the optical absorption cross sections of the precursor materials. Materials are generally classified into their optical band gaps and electronic structures (Figure 2c). Carbonaceous materials (CNFs, rGO, and CB) and black oxides (e.g., Fe_3O_4, Co_3O_4, CuO, and black TiO_2) exhibit high absorbance across the visible-to-infrared spectrum. This broad-spectrum absorption allows carbon materials to serve as efficient "heaters". In continuous form, they can also be used as freestanding heaters with uniform temperature distribution.[13] Therefore, by combining carbonaceous materials and black oxides, one can design hybrid architectures that leverage both intense light absorption and efficient electrical heating, thereby enabling highly controllable flash thermal treatments over large areas or complex geometries. Although stoichiometric wide-bandgap oxides (SnO_2, ZnO, white TiO_2, E_a > 3 eV) are typically poor absorbers of visible light, their photothermal efficiency can be dramatically enhanced through defect engineering.[12,28,29] Even for the same oxide composition, reducing the grain size can modify not only the effective band gap but also the thermal transport properties. A smaller grain size increases the density of grain boundaries, which act as strong phonon-scattering centers, thereby suppressing thermal conductivity. As a result, reduced heat dissipation during IPL generates strong local thermal confinement, enabling intense heating and rapid quenching within milliseconds. This ultrafast process permits high-temperature treatment of carbonaceous materials in ambient air while suppressing decomposition, preserving the phases and structures of metal oxide, and minimizing degradation, such as surface area loss.

2.3. Temperature Measurement Techniques

Precise thermal profiling is a prerequisite for controlling the kinetic pathways of FTS processes. However, quantifying the transient temperature profiles under millisecond-scale irradiation presents a significant metrological challenge. Conventional contact-based thermometry (e.g., thermocouples) is hindered by significant thermal inertia and limited temporal resolution (>100 ms), rendering it incapable of capturing the rapid heating and cooling rates characteristic of FTS.[30] Consequently, high-speed noncontact infrared (IR) pyrometry has been established as the standard for in situ monitoring.[12,26] To accommodate the broad dynamic temperature range of FTS and the abrupt thermal transitions, a single detector is often insufficient. Therefore, a dual-spectral IR sensor system is frequently employed. For instance, a setup might integrate a low-temperature sensor (473−1773 K, detection at $\lambda \approx 2.3$ μm) and a high-temperature sensor (773−3273 K, detection at $\lambda \approx 1.5$ μm). The analog signals from these sensors are converted into digital thermal profiles using a high-speed Data Acquisition (DAQ) board, providing a temporal resolution of 5 μs. Furthermore, the emissivity (ε_λ) evolves dynamically during the flash pulse due to phase transformations, such as the reduction of GO to rGO or the crystallization of amorphous domains.[12,26] The true temperature T is derived from the measured equivalent blackbody temperature $T_{measured}$ using a correction based on Planck's law:

$$\frac{1}{T_{measured}} = \frac{1}{T_{corrected}} + \lambda_{detect} \times \ln \frac{\varepsilon_{measured}}{\varepsilon_{corrected}} \times \frac{1}{C_2}$$

where C_2 is the second radiation constant (14388 μmK^{-1}), λ_{detect} is the detector wavelength, and $\varepsilon_{corrected}$ is the calibrated emissivity of the target material. This rigorous thermometry allows for the precise correlation of thermal history, specifically the measured temperature ($T_{measured}$) and cooling rate ($\frac{dT}{dt}$).

3. FLASH THERMAL-SHOCK SYNTHESIS OF ADVANCED CATALYSTS

3.1. Atomic-Level Engineering Strategies: Heteroatom Doping and Single Atom Catalyst Design

Conventional sintering often suffers from a trade-off: the high temperatures required for phase transformation also accelerate grain coarsening.[31] By reducing the heating duration from hours to milliseconds, the synthesis regime shifts from thermodynamic growth to kinetic constraint.[32] FTS applies high temperatures for ultrashort durations, thereby suppressing diffusion-driven grain coarsening while generating steep thermal gradients that induce lattice strain and defect formation, thereby enabling robust anchoring of mobile metal atoms.[12,31]

The functionalization of carbon supports with heteroatoms (e.g., B, N, P) is a proven strategy to modulate electronic structures and create active sites.[33] However, incorporating these atoms into the rigid sp^2 carbon network requires high activation energy, whereas FTS enables this in ambient air with a low thermal budget, unlike conventional furnace annealing that requires inert atmospheres and prolonged heating.[34] Cha

https://doi.org/10.1021/accountsmr.6c00058
Acc. Mater. Res. XXXX, XXX, XXX−XXX

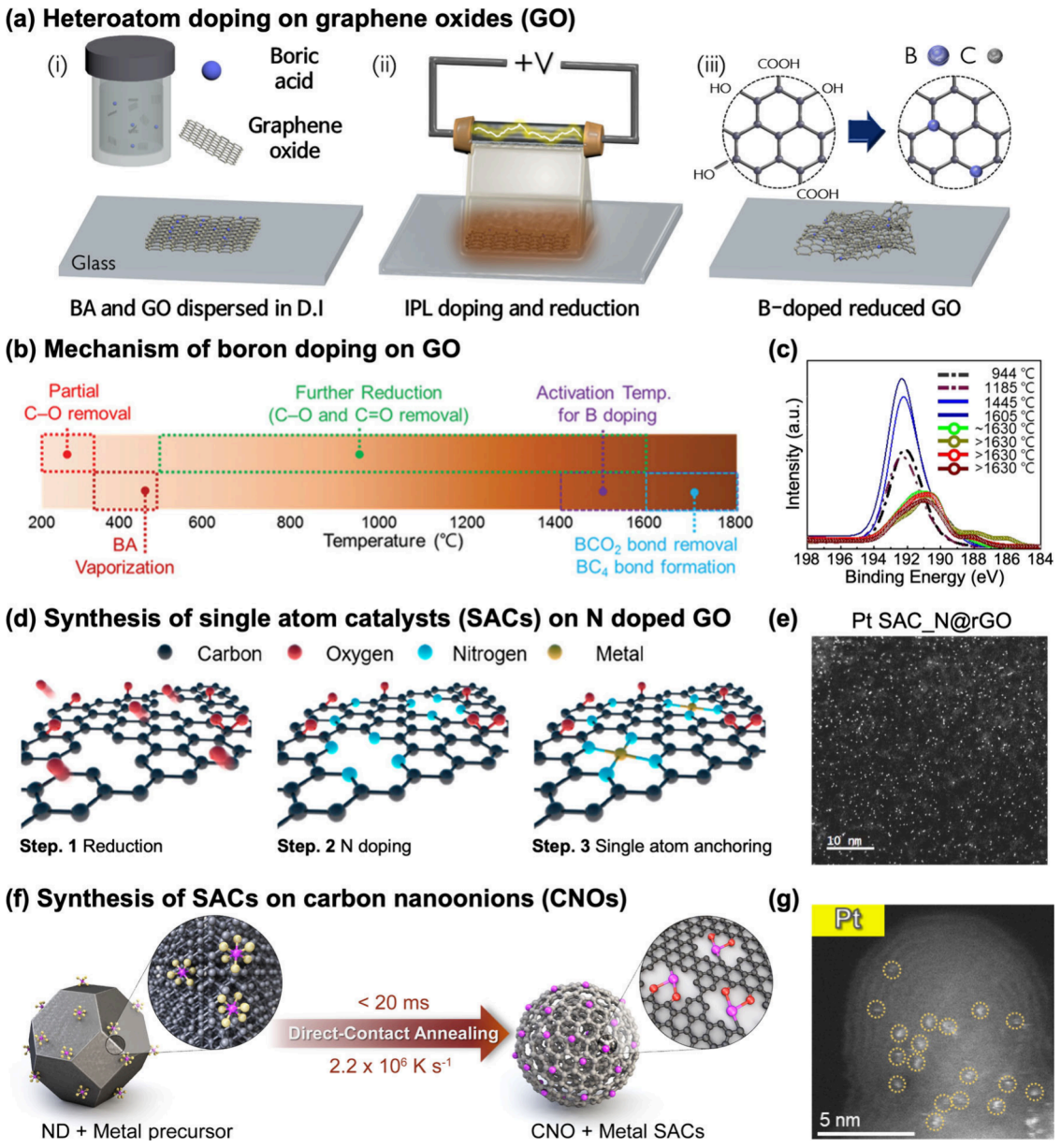

Figure 3. FTS of advanced catalyst (atomic scale). (a) Schematic of the ambient-air synthesis of B@rGO using a single flash pulse. (b) Temperature-affected sequential reactions mechanism of BA@GO. (c) Normalized B 1s XPS spectra depending on the photothermal temperatures. Reproduced with permission from ref 34. Copyright 2020 Wiley. (d) Schematic of the synthesis mechanism of SA_N@rGO. (e) HAADF-STEM image of isolated Pt single atoms on the N-doped graphene. Reproduced with permission from ref 20. Copyright 2023 American Chemical Society. (f) Schematic of the direct-contact annealing (DCA) strategy, transforming NDs into CNOs while simultaneously anchoring single atoms. (g) HAADF-STEM image of Pt_1/CNOs. Reproduced with permission from ref 26. Copyright 2025 American Chemical Society.

et al. demonstrated that boron-doped reduced graphene oxide (B@rGO) can be synthesized via a single flash irradiation (<10 ms) of a GO and boric acid mixture (Figure 3a). The mechanism relies on GO photothermal response, which serves as a localized heat source. Upon irradiation, the high heating (5.30×10^5 K s^{-1}) and cooling (4.57×10^4 K s^{-1}) rates trigger the simultaneous deoxygenation of GO and the thermal decomposition of boric acid (Figure 3b). The high-energy environment facilitates the overcome of the activation barrier for substituting carbon atoms with boron, resulting in the formation of BC_3, BC_2O, and BCO_2, enabling the precise tuning of these doping sites by modulating the irradiation energy (Figure 3c). The ultrafast processing time prevents the combustion of the carbon lattice even in air, preserving the structural integrity while achieving high doping levels (~ 3.6 at %), representing a 10^6-fold reduction in thermal budget compared to traditional methods, establishing FTS as a scalable route for heteroatom engineering. To demonstrate the practical utility of this atomic-level heteroatom doping strategy, they employed the synthesized B@rGO as a sensing layer for room-temperature NO_2 detection. B@rGO yielded superior sensing capabilities, exhibiting a 3.1-fold higher response to 10 ppm of NO_2 relative to pristine rGO and achieving a detection limit as low as 100 ppb.

Beyond heteroatom doping, FTS enables SAs synthesis by forming nitrogen-doped anchoring sites that trap mobile metal atoms during rapid cooling and prevent agglomeration. Kim et al. established a universal protocol for synthesizing high-

https://doi.org/10.1021/accountsmr.6c00058
Acc. Mater. Res. XXXX, XXX, XXX−XXX

density SAs (Co, Ni, Pt) on N-doped graphene (Figure 3d).[20] By flash-irradiating a mixture of metal precursors and melamine on GO, the process induces a cascade of reactions within milliseconds: reduction of GO, decomposition of melamine to form N-doped defects, and the trapping of metal atoms into M-N_x coordination sites. The high temperature (>3000 K) ensures the complete dissociation of metal precursors into isolated atoms, while the subsequent cooling rate (10^5 K s^{-1}) kinetically freezes these atoms into the thermodynamically favorable N-doped graphene before they can diffuse and nucleate into clusters, as visualized by HAADF-STEM (Figure 3e). Substantiating the efficacy of this synthesis platform, the authors evaluated bifunctional capabilities of the engineered SAs across diverse sensing and electrochemical applications. The atomically dispersed Ni active sites of Ni SAs_N@rGO significantly enhanced interaction with NO_2 molecules, yielding a 9.6-fold increase in sensitivity compared to pristine rGO and accelerating adsorption/desorption kinetics, thereby demonstrating that FTS can effectively tailor active centers for specific surface-limited reactions. Furthermore, Co SAs_N@rGO demonstrated remarkable electrocatalytic efficiency for the oxygen reduction reaction in alkaline media, exhibiting a dominant four-electron transfer pathway and superior reaction kinetics. The robust confinement of Co atoms within the N-doped lattice ensured exceptional durability, maintaining its half-wave potential with negligible decay even after 10000 cycling tests.

Recent advancements have further expanded FTS to the synthesis of functionalized high-curvature carbon nanostructures, thereby enhancing catalytic activity through strain effects.[35,36] Jeon et al. introduced a direct-contact annealing (DCA) platform—an extension of the FTS framework—to transform nanodiamonds into carbon nanoonions (CNOs) while simultaneously anchoring 8 different SAs (M_1/CNO, M = Pt, Ru, Ir, Cr, Cu, Co, Ni, Fe) (Figure 3f).[26] By utilizing CB as a photothermal agent to mediate heat transfer, the local temperature is driven up to ∼3030 K in under 20 ms. The DCA process allows simultaneous anchoring of metal atoms to the newly formed, highly curved surfaces (Figure 3g). This approach leverages the nanocurvature of CNOs to modulate the electronic state of the anchored single atoms, yielding superior performance in the hydrogen evolution reaction (HER). Pt_1/CNO exhibited an ultralow overpotential of 13.9 mV at 10 mA cm^{-2} and a mass activity of 2.0 A mg^{-1}_{Pt}, which surpasses commercial Pt/C catalysts by a factor of 5.88. In summary, FTS provides a versatile and energy-efficient platform for atomic-level catalyst design. By manipulating the thermodynamics of bond formation and the kinetics of atomic diffusion, it enables the precise engineering of active sites, ranging from heteroatom dopants to isolated metal atoms, on diverse carbonaceous supports.

3.2. Nanoparticle Functionalization: From Monometallic to Multimetallic Systems

The photothermal effect of metal oxides under FTS is not determined solely by the bandgap but can be widely tuned by microstructure and thermal dissipation, such as crystallite size, defect density, porosity, and thermal conductivity.[12]

Defect- and pore-engineered SnO_2 nanosheets reach ultrahigh temperatures (>2000 K) within 20 ms, exhibiting heating/cooling rates on the order of 10^4–10^5 K s^{-1}, thereby enabling ultrafast phase engineering and catalyst functionalization. Notably, this platform enabled the ultrafast formation and stabilization of noble metals (Pt, Ru, and Ir) and Pt-based alloy NPs on oxide nanosheets (Figure 4a). Owing to the

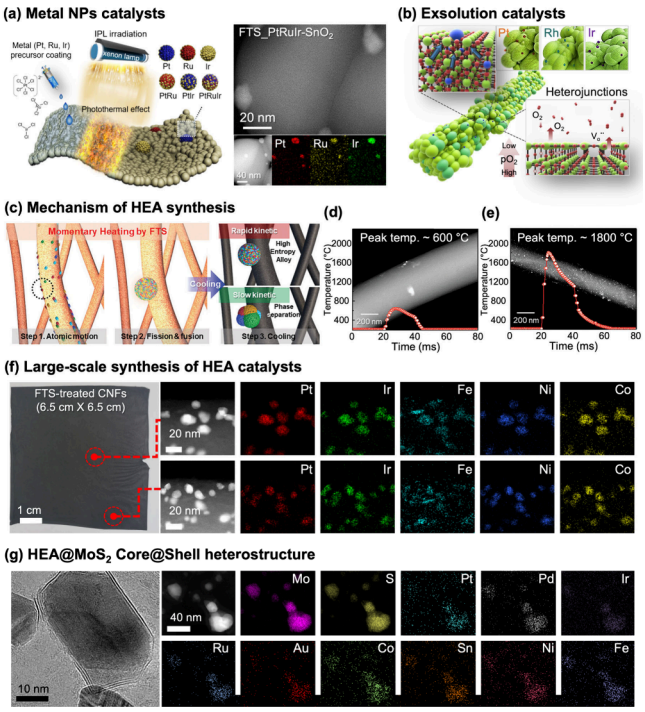

Figure 4. FTS of advanced catalyst (NPs scale). (a) Schematic illustration, HAADF-STEM image, and elemental mapping of PtRuIr-SnO_2. Reproduced with permission from ref 12. Copyright 2022 Elsevier. (b) Schematic of the ambient-air exsolution process on WO_3 nanofibers with Pt, Rh, and Ir NP-socketed heterojunctions. Reproduced with permission from ref 25. Copyright 2022 American Chemical Society. (c) Mechanism of HEA synthesis. (d), (e) Comparison of HEA formation on CNF at different temperatures. (f) Photograph of a large-scale HEA-loaded CNF and HAADF-STEM images with EDS mapping of PtIrFeNiCo quinary alloy. Reproduced with permission from ref 13. Copyright 2023 Wiley. (g) HAADF-STEM image and corresponding EDS mapping of a HEA@MoS_2 core@shell heterostructure. Reproduced with permission from ref 24. Copyright 2025 Wiley.

millisecond-scale heating, catalysts can be decorated in a small and uniform distribution, enhancing chemical/electronic sensitization effects in chemiresistive sensing. Pt-based binary/ternary catalysts on SnO_2 nanosheets exhibited tunable selectivity toward volatile sulfur-containing molecules (e.g., H_2S, and C_2H_6S). The highly active alloy catalysts preferentially promoted oxidation of H_2S, thereby improving selectivity toward C_2H_6S.

Beyond NP decoration, FTS can also trigger rapid oxygen loss and oxygen-vacancy formation, producing reduced oxide domains and heterojunctions that strongly modulate electrical transport. These oxygen vacancies also act as a key thermochemical driver of dopant reduction and surface segregation (i.e., exsolution).[37] Shin et al. demonstrated ultrafast ambient-air exsolution of Pt, Rh, and Ir on WO_3 nanofibers by FTS, completing exsolution within ∼20 ms (Figure 4b).[25] The ultrashort processing time minimizes support degradation and expands the practical exsolution support materials. The FTS also induced partial surface reduction, forming WO_{3-x}/WO_3 heterojunctions that substantially improved adsorbed oxygen species and, together with

https://doi.org/10.1021/accountsmr.6c00058
Acc. Mater. Res. XXXX, XXX, XXX−XXX

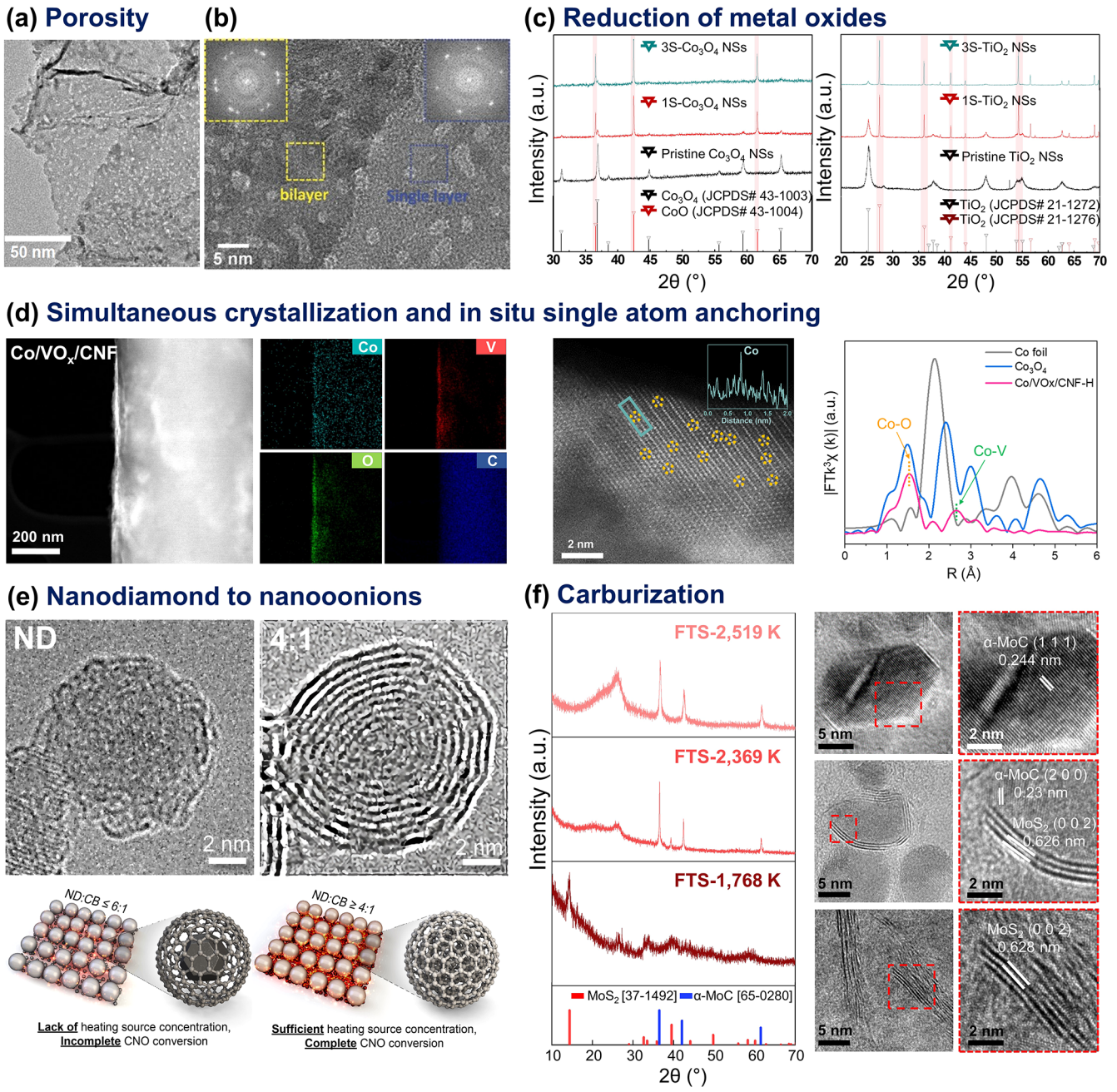

Figure 5. FTS of thermochemical transformations. (a, b) TEM and high-resolution TEM images of FTS of porous 2D RuO_2 nanosheets. Reproduced with permission from ref 44. Copyright 2017 Wiley. (c) XRD patterns demonstrating the reduction and phase transitions of metal oxides; (left) partial reduction of Co_3O_4 to CoO and (right) phase transition of TiO_2 from anatase to rutile. Reproduced with permission from ref 12. Copyright 2022 Elsevier. (d) HAADF-STEM, corresponding EDS mapping, and EXAFS spectra of Co/VO_x/CNF to confirm the simultaneous crystallization and in situ single atom anchoring. Reproduced from ref 47, Royal Society of Chemistry (CC BY 3.0 License). TEM images and schematic illustration of the DCA strategy for CNO synthesis, highlighting that an optimized ratio of ND to CB is critical to concentrate photothermal heat. Reproduced with permission from ref 26. Copyright 2025 American Chemical Society. (f) XRD patterns and corresponding high-resolution TEM images showing temperature-dependent phase control in Mo-based systems; by tuning the FTS temperature, the product can be selectively engineered from MoS_2 to metastable α-MoC via carbothermal reactions. Reproduced with permission from ref 24. Copyright 2025 Wiley.

socketed exsolved NPs, enhanced gas-sensing performance. As a representative outcome, the Pt exsolution NPs on WO_3 NFs exhibited response (R_{air}/R_{gas}) > 800 for 1 ppm of H_2S at 80% relative humidity and 623 K. They maintained stable sensing over >200 cycles toward 1 ppm, consistent with the sintering stability expected from socketed exsolution geometries.

The high-temperature profile is advantageous for the synthesis of high-entropy materials.[32] However, preserving a highly distorted atomic configuration requires precise kinetic control to inhibit diffusion-driven segregation. Solid-state diffusion is significantly slower, dropping to ~10^3 nm s^{-1} near the melting point and drastically lower (~1 nm s^{-1}) at half the melting temperature.[38] Therefore, achieving control-

https://doi.org/10.1021/accountsmr.6c00058
Acc. Mater. Res. XXXX, XXX, XXX−XXX

lable synthesis, such as forming metal NPs with high loading, requires the precise utilization of short heating pulses within a diffusion-constrained environment. FTS could provide high temperatures, where the configurational entropy contribution to the Gibbs free energy ($\Delta G_{mix} = \Delta H_{mix} - T\Delta S_{mix}$) becomes sufficiently larger that the $-T\Delta S_{mix}$ term than the enthalpy of mixing (ΔH_{mix}). This thermodynamic regime enables the formation of single-phase solid solutions from highly immiscible elements.[39] Therefore, the subsequent ultrafast quenching "freezes" this high-entropy state, stabilizing highly distorted atomic configurations that would otherwise undergo phase separation under equilibrium cooling conditions.

Cha et al. demonstrated FTS of high-entropy alloy (HEA) NPs on carbon-based supports (carbon nanofibers (CNFs), MXenes, and graphene oxide(GO)), where ultrafast heating drives elemental interdiffusion, repeated fission-fusion events, and subsequent quenching stabilizes mixed phases.[13] Notably, phase separation was suppressed only when sufficiently high temperatures and rapid cooling rates were ensured (Figure 4c). They further showed that processing temperature strongly affects alloy uniformity because carbon-supported formation can be coupled with carbothermal reactions that require sufficient activation energy (Figures 4d,e). In addition, it is well-suited for large-area FTS processing in a noncontact manner, since the xenon-flash IPL inherently delivers broadband, high-intensity illumination over a large area. Cha et al. processed a 6.0 × 6.0 cm^2 CNF membrane using a 15 cm lamp (with a beam reflector), achieving uniform HEA NP formation across both the center and the edge of the membrane, highlighting the scalability of IPL-driven FTS toward high-throughput production (Figure 4f). In this approach, Pt and Ir are alloyed with transition metals (Fe, Ni, and Co) to form HEA catalysts. These HEAs provide an increased density of active sites and strengthened adsorption energetics, leading to enhance HER activity. Notably, Ce incorporation in PtIrFeNiCoCe@CNF is associated with markedly improved durability, with stable performance maintained over 5000 cycles, attributed to enhanced electronic modulation and suppressed Ir dissolution. Overall, FTS offers a broadly composition-flexible platform, enabling HEA NPs to be formulated with application-selected elements.

FTS not only enables ultrafast HEA synthesis but also facilitates HEA-based heterostructure engineering, including conformal encapsulation with layered shells. Such shells can enhance sintering resistance via confinement and can further modulate catalytic activity when curvature- or strain-induced electronic effects are introduced. By reaching >3000 K within ~ 10 ms with GO as a photothermal agent, FTS provides sufficient nonequilibrium thermal input to overcome interfacial barriers and enable encapsulation. The FTS suppresses excessive lateral growth that typically produces undesirable morphologies, thereby favoring conformal core@shell architectures. In this framework, HEA cores, such as PtPdIrRuAuCoSnNiFeCu, can be uniformly synthesized and then encapsulated by a MoS_2 shell when a MoS_2 precursor (e.g., ammonium tetrathiomolybdate, ATTM) is added to the GO-containing precursor mixture (Figure 4g).[24] Rapid quenching after the milliseconds annealing step suppresses diffusion-driven overgrowth, enabling nanoscale, conformal HEA@MoS_2 heterostructures.

4. FLASH THERMAL-SHOCK SYNTHESIS OF THERMOCHEMICAL TRANSFORMATIONS

4.1. Porosity Generation and Phase Reconstruction

Surface restructuring via thermal treatment is an efficient strategy to modulate the electronic structure and catalytic activity of nanomaterials.[40,41] Porous architectures are highly desirable for chemical sensing because they promote gas transport into the sensing layer and increase the accessible surface area for reaction.[42,43] However, introducing well-defined nanopores into atomically thin oxides is challenging because conventional thermal pore-forming routes often lead to agglomeration and offer limited control over pore size and density at the sub-10 nm scale. Choi et al. used IPL-driven FTS to generate abundant sub-5 nm pores (average pore size ≈ 2.58 ± 1.16 nm) in 2D RuO_2 nanosheets on a flexible Ag nanowire-embedded colorless polyimide (Ag NW-cPI) platform while preserving the hexagonal crystal framework under a 15 ms pulse. (Figure 5a,b).[44] The millisecond-scale FTS enabled pore engineering without thermally degrading the substrate. Pore formation is attributed to IPL-induced RuO_2 oxidation and dehydration of hydrated Ru oxides, which releases water and creates voids. Temperature-controlled operation using the Ag NW-cPI heater accelerated NO_2 reaction kinetics, yielding approximately 1.94-fold faster adsorption and 3.5-fold faster desorption when the film temperature increased from 314.9 to 353.3 K, enabling a wearable, patch-type NO_2 sensor demonstration.

The ultrafast photothermal pulse instantaneously elevates the surface temperature, which can create a locally oxygen gradient (i.e., effective oxygen partial pressure gradient) at the oxide/air interface and promote lattice-oxygen release, thereby generating oxygen vacancies.[45,46] Subsequent millisecond-scale quenching kinetically traps these nonequilibrium defect states at room temperature; when the reduction is sufficiently strong, it can proceed beyond point defects to a partial phase transition into lower-valence oxides (e.g., SnO_2 to SnO, Co_3O_4 to CoO) (Figure 5c). Moreover, TiO_2 can undergo a substantial anatase-to-rutile transition by tuning the FTS conditions, enabling phase-selective engineering via precisely controlled ultrafast thermal energy.

Furthermore, the FTS induces a high concentration of oxygen vacancies, which serve as binding sites to stabilize single atoms in low-coordination environments. Jeon et al. employed FTS to simultaneously crystallize amorphous vanadium oxide and anchor Co single atoms into generated oxygen vacancies (Co/VO_x/CNF) (Figure 5d).[47] As illustrated in the HAADF-STEM and EDS mapping images, the FTS triggers an instantaneous atomic rearrangement that transforms the amorphous layer into a highly ordered crystalline phase while kinetically trapping Co atoms. The Fourier-transformed Co K-edge extended X-ray absorption fine structure (EXAFS) confirms a unique splitting of the first coordination shell into two distinct paths: a short Co−O1 and a long Co−O2 interaction. This coordination splitting is a direct consequence of the presence of a defect-trapped state, where the Co atom is firmly anchored within a lattice vacancy. This configuration results in a reduced coordination number and a nonuniform local symmetry, thereby optimizing the electronic environment for the oxygen evolution reaction (OER).

Direct-contact annealing (DCA) process-enabled by FTS triggers the phase transformation of sp^3 diamond cores into

https://doi.org/10.1021/accountsmr.6c00058
Acc. Mater. Res. XXXX, XXX, XXX−XXX

Table 2. Summary of Diverse Nanomaterial Design Strategies Achieved via IPL-Driven FTS, Highlighting Substrate Types, Results, Processing Parameters, and Applications

Nanosubstrate	Adding	Result	Temperature (measured)	Process time	Energy density	Application	Ref.
Carbon black (carbon)	Nanodiamond/Metal ions	Phase engineering/SACs	~2760 °C	<20 ms	40 J/cm^2	HER	26
Carbon nanofiber (carbon)	Metal ions (Pt, Ir, Fe, Ni, Co)	HEAs	~1800 °C	<20 ms	4.9 J/cm^2	HER, OER	13
Carbon nanofiber (carbon)	Vanadium oxide/Metal ions (Co, Pt, Ru, Cu)	Phase engineering/SACs	~1600 °C	<20 ms	8, 10 J/cm^2	OER	47
Graphene (carbon)	Ag nanowires	Welding	N/A	<20 ms	33 J/cm^2	Transparent conductive electrode	50
Graphene oxide (carbon)	Doping source (nitrogen)/ Metal ions	SACs	~2850 °C	<10 ms	10.7 J/cm^2	Gas sensors (NO_2) OER	20
Graphene oxide (carbon)	Metal ions (Mo, W, S)	Core−shell NPs/ Metastable carbides	~2900 °C	<10 ms	10, 25 J/cm^2	Gas sensor (NO_2) HER	24
Graphene oxide (carbon)	Doping source (boron)	Heteroatom doping	~1650 °C	<10 ms	11.1−31.3 J/cm^2	Gas sensors (NO_2)	34
Graphene oxide (carbon)	N/A	Reduction	~490 °C	<15 ms	1.15 J/cm^2	Gas sensor (H_2S, EtOH, H_2)	49
SnO_2 nanosheet (oxide)	Metal ions (Pt, Ru, Ir)	Phase engineering/ Ternary NPs	~1800 °C	<20 ms	6.4−21.7 J/cm^2	Gas sensor (H_2S, CH_3SH)	12
WO_3 nanofiber (oxide)	Doping source (Pt, Rh, Ir)	Exsolution NPs	~1300 °C	<20 ms	20 J/cm^2	Gas sensor (H_2S)	25
RuO_2 (oxide)	N/A	Pore structures	N/A	<15 ms	1.15 J/cm^2	Gas sensor (NO_2)	44

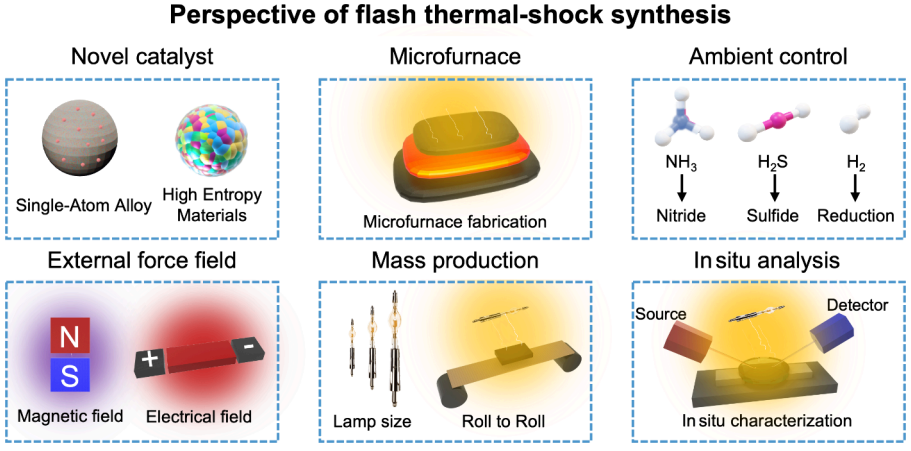

Figure 6. Perspective of IPL-driven FTS.

concentric graphitic shells (sp^2). During this reconstruction, metal precursors dispersed in the mix are trapped as single atoms on the newly formed, highly curved fullerene-like surfaces (Figure 5e).[26] Jeon et al. systematically investigated the impact of the nanodiamond to CB ratio on this restructuring process. FTS provides the necessary energy to break the metastable sp^3 C−C bonds of the diamond lattice, driving the surface reconstruction into the thermodynamically stable sp^2 graphitic phase. Unlike slow annealing, which produces planar graphite sheets, the ultrafast cooling rate (2.2×10^6 K s^{-1}) of FTS kinetically traps the graphitic layers into concentric, high-curvature shells, resulting in the formation of carbon nanoonions (CNOs). This surface restructuring is not merely morphological; the high curvature induces significant lattice strain, which modulates the surface electronic environment, making it an ideal support for anchoring single atoms. As discussed earlier, the high curvature of the CNO shells modulates the electronic states of the anchored Pt atoms while facilitating proton distribution around these active sites, thereby accelerating HER kinetics.

4.2. Carbothermic Reaction for Heterostructure Formation

FTS engineering is not limited to metal oxides or carbon materials but can be extended to transition metal dichalcogenides (TMDs) and carbides (TMCs) through GO assisted ultrafast photothermal annealing. The FTS provides sufficient activation energy for interfacial reconstruction and heterostructure formation across diverse material systems, while suppressing excessive growth through rapid quenching, thereby enabling combinations and architectures that are difficult to realize with conventional long-duration thermal treatments. In this approach, the GO-based FTS reaches tunable temperatures (1768−3162 K) within ~10 ms under ambient air, enabling (1) direct TMD formation from precursors above ~1700 K and (2) carbothermic reactions above ~ 2300 K that yield metastable TMCs and core@shell heterostructures (e.g., TMC@TMD and TMC@carbon). Shin et al. demonstrated selective synthesis of phase-engineered MoS_2 (2H-rich at 1768 K; mixed 1T/2H at 2369 K; 1T-rich at 2519 K), as well as metastable α-MoC and α-MoC@MoS_2 core@shell nanoparticles on rGO by controlling the photothermal temperature (Figure 5f).[24] Similar phase- and heterostructure-engineering

https://doi.org/10.1021/accountsmr.6c00058
Acc. Mater. Res. XXXX, XXX, XXX−XXX

was extended to W-based systems, including metastable 1T-WS_2 and tungsten carbide/oxycarbide products. These phase- and heterostructure-controlled nanocomposites exhibited high performance as gas sensors and HER catalysts. For gas sensors, α-MoC@MoS_2/rGO exhibited 9.2-fold higher NO_2 response (5 ppm) than pristine rGO at 80% relative humidity. For electrocatalysis, W_2CO/rGO delivered an HER overpotential of 50.5 mV (η_{10}) with a 65.7 mV dec^{-1} Tafel slope, indicating rapid kinetics relative to the other W-based composites in that study.

5. CONCLUSIONS AND PERSPECTIVE

As highlighted throughout this Account, IPL-driven FTS provides a versatile nonequilibrium platform for nanomaterial design. At the atomic level, FTS enables heteroatom doping and single-atom stabilization under ultrafast, low-thermal-budget conditions. At the nanoscale, the ultrafast thermal input drives rapid nanoparticle functionalization, including the formation of multimetallic and high-entropy architectures. Beyond compositional control, FTS also enables porosity generation and phase reconstruction, allowing selective defect formation, metastable phase stabilization, and surface restructuring. Furthermore, through carbothermic reactions, FTS extends its synthetic scope to heterostructure formation, enabling rapid formation of TMD- and TMC-based hybrid nanostructures. As comprehensively summarized in Table 2, IPL-driven FTS has been successfully adapted across a broad spectrum of applications.

In this Perspective, we highlight key research directions that will accelerate the development of FTS and define its future evolution as a platform for innovative materials synthesis (Figure 6). **(1) Expanding the accessible compositional and structural space**. A primary feature of FTS is the broadening of structural and compositional materials under nonequilibrium conditions. FTS is well-positioned to broaden the structural and compositional landscapes of materials by accelerating the synthesis of single-atom alloys, high-entropy oxides, and complex heterostructures that are otherwise difficult to access via conventional thermal annealing. **(2) Microfurnace/absorber engineering for nonphotothermal substrates**. To expand FTS beyond photothermal materials, absorber engineering will be essential for substrates with low absorption, including wide-bandgap, reflective, and transparent materials. Practical approaches include photothermal coatings, sacrificial absorbers, plasmonic structures, and black interlayers that localize heat at the target interface during FTS. **(3) Atmosphere programming to access mixed-anion and nonoxide chemistries**. Expanding FTS beyond ambient processing by using controlled reaction atmospheres, such as tunable oxygen partial pressure, humidity, and reactive gases, offers a major opportunity to access nitrides, sulfides, oxynitrides, and other mixed-anion phases via single-step nonequilibrium pathways. For example, flashlamp implementations under glovebox and inert-atmosphere conditions enable new atmosphere-sensitive processing routes for battery applications. **(4) Hybrid heating profiles as a new degree of freedom.** Coupling FTS with additional external fields, such as direct Joule heating or induction heating, can generate hybrid spatiotemporal heating profiles (e.g., simultaneous volumetric heating combined with surface-localized thermal shock), thereby offering more precise control over phase transformations, defect generation, and interface reactions than any single modality alone. **(5) Process engineering and scale-up: from lab to manufacturing architectures.** Beyond laboratory-scale demonstrations, large-scale production will require larger lamp systems, roll-to-roll processing, and robotics-enabled automation. Together with precise control of energy uniformity, synchronization of xenon pulse frequency with web speed, and robust thermal management to minimize lamp degradation, these advances will be essential for ensuring a consistent thermal history and uniform material quality across large-area substrates. **(6) Millisecond-resolved in situ/operando analysis.** A key bottleneck in FTS is the limited mechanistic understanding of transformations occurring during the millisecond flash event. In particular, how wavelength and temporal energy-delivery profiles govern reduction, phase transition, nucleation, and defect formation remains unclear. Resolving this will require synchronized in situ/operando platforms, including time-resolved optical spectroscopy, quadrupole mass spectrometry, gas chromatography–mass spectrometry, and time-resolved X-ray techniques.

In closing, this Account establishes IPL-driven FTS as a powerful nonequilibrium platform for nanomaterials design, capable of accessing heterointerface nanostructures, metastable, and advanced functionalities far beyond conventional thermodynamic limits. We anticipate that continued advances in process control, scale-up strategies, and mechanistic understanding will enable FTS to play a central role in the rational design of next-generation nanomaterials. We hope that this Account provides a useful framework and inspiration for scientists and researchers seeking to harness ultrafast FTS for impactful and broad applications in nanoscience and innovative materials engineering.

AUTHOR INFORMATION

Corresponding Author

Il-Doo Kim − *Department of Materials Science and Engineering, Korea Advanced Institute of Science and Technology (KAIST), Daejeon 34141, Republic of Korea;* orcid.org/0000-0002-9970-2218; Email: idkim@kaist.ac.kr

Authors

Euichul Shin − *Department of Materials Science and Engineering, Korea Advanced Institute of Science and Technology (KAIST), Daejeon 34141, Republic of Korea*

Dogyeong Jeon − *Department of Materials Science and Engineering, Korea Advanced Institute of Science and Technology (KAIST), Daejeon 34141, Republic of Korea*

Hamin Shin − *Human-centered Sensing Laboratory, Department of Mechanical and Process Engineering, ETH Zurich, Zurich CH-8092, Switzerland;* orcid.org/0000-0001-8330-5448

Jun-Hwe Cha − *School of Electrical Engineering, Korea Advanced Institute of Science and Technology, Daejeon 34141, Republic of Korea*

Complete contact information is available at: https://pubs.acs.org/10.1021/accountsmr.6c00058

Author Contributions

#E.S. and D.J. contributed equally to this work.

Notes

The authors declare no competing financial interest.

https://doi.org/10.1021/accountsmr.6c00058
Acc. Mater. Res. XXXX, XXX, XXX−XXX

Biographies

Euichul Shin is a Postdoctoral researcher at KAIST. He received his Ph.D. degree from KAIST under the supervision of Prof. Il-Doo Kim. His research focuses on the structural engineering of functional nanomaterials via photothermal treatments for gas-sensing and electrocatalytic applications.

Dogyeong Jeon is a Ph.D. candidate at KAIST. Her research focuses on the development of atomically engineered nanomaterials for electrocatalytic systems and advanced biosensing platforms.

Hamin Shin is a Postdoctoral researcher at ETH Zurich under the supervision of Prof. Andreas Güntner, and he received his Ph.D. from KAIST under the supervision of Prof. Il-Doo Kim. His research focuses on the synthesis and operando characterization of atomic-level active sites in catalysts, for chemiresistive gas sensors and various catalytic reactions.

Jun-Hwe Cha is a researcher at SK hynix. He received his Ph.D. degree from KAIST under the supervision of Prof. Sung-Yool Choi. His research focuses on the photonic/optical annealing and device engineering of low-dimensional materials, including memristors and neuromorphic devices, as well as related electronic applications.

Il-Doo Kim is a Chair Professor in the Department of Materials Science and Engineering (DMSE) at KAIST. He received his Ph.D. in DMSE from KAIST and conducted postdoctoral research at MIT from 2003 to 2005. Before his position at KAIST, he worked as a senior research scientist at the Korea Institute of Science and Technology (KIST) from 2005 to 2011. His research focuses on functional organic and inorganic nanomaterials with controlled structural features for sustainable membrane technology, energy harvesting, storage systems, and chemical sensors.

■ ACKNOWLEDGMENTS

This work was supported by National Research Foundation of Korea (NRF) grant funded by the Korean government (MSIT) (Nos. RS-2024-00435493, RS-2023-00236572). This work was supported by the National Research Foundation of Korea grant funded by the Korea government, Ministry of Science and ICT (Development of Nanofiber Yarn Based Compound Sensor as a Comprehensive Wearable Healthcare Solution) (Grant No. RS-2024-00357296).

■ REFERENCES

(1) Ayuk, E.; Ugwu, M.; Aronimo, S. B. A review on synthetic methods of nanostructured materials. *Chem. Res. J.* **2017**, *2* (5), 97−123.
(2) Zaera, F. Nanostructured materials for applications in heterogeneous catalysis. *Chem. Soc. Rev.* **2013**, *42* (7), 2746−2762.
(3) Bulemo, P. M.; Kim, D.-H.; Shin, H.; Cho, H.-J.; Koo, W.-T.; Choi, S.-J.; Park, C.; Ahn, J.; Guntner, A. T.; Penner, R. M.; Kim, I.-D. Selectivity in Chemiresistive Gas Sensors: Strategies and Challenges. *Chem. Rev.* **2025**, *125* (8), 4111−4183.
(4) Hu, X.; Zuo, D.; Cheng, S.; Chen, S.; Liu, Y.; Bao, W.; Deng, S.; Harris, S. J.; Wan, J. Ultrafast materials synthesis and manufacturing techniques for emerging energy and environmental applications. *Chem. Soc. Rev.* **2023**, *52* (3), 1103−1128.
(5) Zou, J.; Tang, L.; Kang, L. Innovative Heating for the Nano Age: Exploring the Potentials of Carbothermal Shock. *ACS Nano* **2025**, *19* (1), 152−186.
(6) Kim, M.; Kim, Y.; Ha, M. Y.; Shin, E.; Kwak, S. J.; Park, M.; Kim, I.-D.; Jung, W. B.; Lee, W. B.; Kim, Y.; Jung, H.-T. Exploring optimal water splitting bifunctional alloy catalyst by pareto active learning. *Adv. Mater.* **2023**, *35* (17), 2211497.
(7) Xie, H.; Liu, N.; Zhang, Q.; Zhong, H.; Guo, L.; Zhao, X.; Li, D.; Liu, S.; Huang, Z.; Lele, A. D.; Brozena, A. H.; Wang, X.; Song, K.; Chen, S.; Yao, Y.; Chi, M.; Xiong, W.; Rao, J.; Zhao, M.; Shneider, M. N.; Luo, J.; Zhao, J.-C.; Ju, Y.; Hu, L. A stable atmospheric-pressure plasma for extreme-temperature synthesis. *Nature* **2023**, *623* (7989), 964−971.
(8) Zhong, G.; Xu, S.; Chen, C.; Kline, D. J.; Giroux, M.; Pei, Y.; Jiao, M.; Liu, D.; Mi, R.; Xie, H.; Yang, B.; Wang, C.; Zachariah, M. R.; Hu, L. Synthesis of metal oxide nanoparticles by rapid, high-temperature 3D microwave heating. *Adv. Funct. Mater.* **2019**, *29* (48), 1904282.
(9) Zhang, D.; Gokce, B.; Barcikowski, S. Laser synthesis and processing of colloids: fundamentals and applications. *Chem. Rev.* **2017**, *117* (5), 3990−4103.
(10) Choi, S.-J.; Yu, H.; Jang, J.-S.; Kim, M.-H.; Kim, S.-J.; Jeong, H. S.; Kim, I.-D. Nitrogen-doped single graphene fiber with platinum water dissociation catalyst for wearable humidity sensor. *Small* **2018**, *14* (13), 1703934.
(11) Choi, S.-J.; Kim, S.-J.; Kim, I.-D. Ultrafast optical reduction of graphene oxide sheets on colorless polyimide film for wearable chemical sensors. *NPG Asia Mater.* **2016**, *8* (9), e315−e315.
(12) Kim, D.-H.; Cha, J.-H.; Shim, G.; Kim, Y. H.; Jang, J.-S.; Shin, H.; Ahn, J.; Choi, S.-Y.; Kim, I.-D. Flash-thermochemical engineering of phase and surface activity on metal oxides. *Chem.* **2022**, *8* (4), 1014−1033.
(13) Cha, J. H.; Cho, S. H.; Kim, D.-H.; Jeon, D.; Park, S.; Jung, J. W.; Kim, I.-D.; Choi, S.-Y. Flash-thermal shock synthesis of high-entropy alloys toward high-performance water splitting. *Adv. Mater.* **2023**, *35* (46), 2305222.
(14) Tao, X.-S.; Chu, F.; Wang, S.; Fang, X.; Zhang, J.; Meng, J.; Sha, J.; Chen, Y. Advances in high-temperature shock technology for structural engineering of electrode materials: a review. *Energy Z.* **2025**, *1* (1), 100003.
(15) Cui, X.; Ruan, Q.; Zhuo, X.; Xia, X.; Hu, J.; Fu, R.; Li, Y.; Wang, J.; Xu, H. Photothermal nanomaterials: a powerful light-to-heat converter. *Chem. Rev.* **2023**, *123* (11), 6891−6952.
(16) Brongersma, M. L.; Halas, N. J.; Nordlander, P. Plasmon-induced hot carrier science and technology. *Nat. Nanotechnol.* **2015**, *10* (1), 25−34.
(17) Matter, M. E.; Čamdžić, L.; Stache, E. E. Photothermal conversion by carbon black facilitates aryl migration by photon-promoted temperature gradients. *Angew. Chem., Int. Ed.* **2023**, *62* (40), No. e202308648.
(18) Dreyer, D. R.; Park, S.; Bielawski, C. W.; Ruoff, R. S. The chemistry of graphene oxide. *Chem. Soc. Rev.* **2010**, *39* (1), 228−240.
(19) Matter, M. E.; Tagnon, C.; Stache, E. E. Recent applications of photothermal conversion in organic synthesis. *ACS Cent. Sci.* **2024**, *10* (8), 1460−1472.
(20) Kim, D.-H.; Cha, J.-H.; Chong, S.; Cho, S.-H.; Shin, H.; Ahn, J.; Jeon, D.; Kim, J.; Choi, S.-Y.; Kim, I.-D. Flash-thermal shock synthesis of single atoms in ambient air. *ACS Nano* **2023**, *17* (23), 23347−23358.
(21) Gengler, R. Y.; Badali, D. S.; Zhang, D.; Dimos, K.; Spyrou, K.; Gournis, D.; Miller, R. D. Revealing the ultrafast process behind the photoreduction of graphene oxide. *Nat. Commun.* **2013**, *4* (1), 2560.
(22) Yu, X.; Fan, S.; Zhu, B.; El-Hout, S. I.; Zhang, J.; Chen, C. Recent progress on photothermal nanomaterials: Design, mechanism, and applications. *Green Energy Environ.* **2025**, *10* (7), 1377−1436.
(23) Park, J. H.; Pattipaka, S.; Hwang, G.-T.; Park, M.; Woo, Y. M.; Kim, Y. B.; Lee, H. E.; Jeong, C. K.; Zhang, T.; Min, Y.; Park, K.-I.; Lee, K. J.; Ryu, J. Light−Material Interactions Using Laser and Flash Sources for Energy Conversion and Storage Applications. *Nano-Micro Lett.* **2024**, *16* (1), 276.
(24) Shin, E.; Kim, D.-H.; Sagong, M.; Choe, J.; Park, S. H.; Ahn, J.; Baek, J. W.; Kim, M.; Woo, S.; Cho, Y.; Choi, S.-J.; Kim, S.-J.; Yuk, J. M.; Li, J.; Choi, S.-Y.; Kim, I.-D. Flash Thermal Shock Synthesis of Heterostructured Transition Metal Dichalcogenides and Carbides in Milliseconds. *Adv. Mater.* **2025**, *37*, 2419790.

https://doi.org/10.1021/accountsmr.6c00058
Acc. Mater. Res. XXXX, XXX, XXX−XXX

(25) Shin, E.; Kim, D.-H.; Cha, J.-H.; Yun, S.; Shin, H.; Ahn, J.; Jang, J.-S.; Baek, J. W.; Park, C.; Ko, J.; Park, S.; Choi, S.-Y.; Kim, I.-D. Ultrafast ambient-air exsolution on metal oxide via momentary photothermal effect. *ACS Nano* **2022**, *16* (11), 18133−18142.
(26) Jeon, D.; Shin, H.; Cha, J.-H.; Kim, H.; Park, S.; Ahn, J.; Cho, S.-H.; Park, C.; Kim, D.-H.; Shin, E.; Baik, H.; Kim, J.; Choi, S.-Y.; Kim, I.-D. Photothermal Annealing-Enabled Millisecond Synthesis of Carbon Nanoonions and Simultaneous Single-Atom Functionalization. *ACS Nano* **2025**, *19* (38), 34235−34247.
(27) Manzaneda-González, V.; Jenkinson, K.; Peña-Rodríguez, O.; Borrell-Grueiro, O.; Triviño-Sánchez, S.; Bañares, L.; Junquera, E.; Espinosa, A.; González-Rubio, G.; Bals, S.; Guerrero-Martínez, A. From multi-to single-hollow trimetallic nanocrystals by ultrafast heating. *Chem. Mater.* **2023**, *35* (22), 9603−9612.
(28) Shin, J.; Lee, G.; Choi, M.; Jang, H.; Lim, Y.; Kim, G.-S.; Nam, S.-H.; Baek, S.-H.; Song, H.-C.; Kim, J.; Kang, C.-Y.; Lee, J.-O.; Jeon, S.; Cho, D.; Jang, J.-S. Atomically mixed catalysts on a 3D thin-shell TiO_2 for dual-modal chemical detection and neutralization. *J. Mater. Chem. A* **2023**, *11* (34), 18195−18206.
(29) Park, G.; Choi, M.; Choi, H.-J.; Shim, Y.-S.; Kim, S.-J.; Lee, J.-O.; Cho, D. Flash-Induced Thermochemical Heterostructuring of a Nickel Oxide/Zinc Oxide Nanomesh for NO_2 Sensing. *ACS Appl. Nano Mater.* **2025**, *8* (20), 10704−10716.
(30) Biesuz, M.; Karacasulu, L.; Vakifahmetoglu, C.; Sglavo, V. M. On the temperature measurement during ultrafast high-temperature sintering (UHS): Shall we trust metal-shielded thermocouples? *J. Eur. Ceram. Soc.* **2024**, *44* (5), 3479−3485.
(31) Zhou, B.; Liu, K.; Yu, K.; Zhou, Q.; Gao, Y.; Gao, X.; Chen, Z.; Chen, W.; Chen, P. Ultrafast Synthesis of Single-Atom Catalysts for Electrocatalytic Applications. *Small* **2025**, 2501917.
(32) Han, Y.-C.; Cao, P.-Y.; Tian, Z.-Q. Controllable synthesis of solid catalysts by high-temperature pulse. *Acc. Mater. Res.* **2023**, *4* (8), 648−654.
(33) Choi, C. H.; Park, S. H.; Woo, S. I. Binary and ternary doping of nitrogen, boron, and phosphorus into carbon for enhancing electrochemical oxygen reduction activity. *ACS Nano* **2012**, *6* (8), 7084−7091.
(34) Cha, J. H.; Kim, D.-H.; Park, C.; Choi, S.-J.; Jang, J.-S.; Yang, S. Y.; Kim, I.-D.; Choi, S.-Y. Low-thermal-budget doping of 2D materials in ambient air exemplified by synthesis of boron-doped reduced graphene oxide. *Adv. Sci.* **2020**, *7* (7), 1903318.
(35) Chen, C.; Zhang, Z.; Dai, L.; Li, B.; Li, Z. High-curvature single-atom catalysts for electrocatalysis: A review. *Appl. Catal. A: Gen.* **2025**, *694*, No. 120160.
(36) Liu, D.; Li, X.; Chen, S.; Yan, H.; Wang, C.; Wu, C.; Haleem, Y. A.; Duan, S.; Lu, J.; Ge, B.; Ajayan, P. M.; Luo, Y.; Jiang, J.; Song, L. Atomically dispersed platinum supported on curved carbon supports for efficient electrocatalytic hydrogen evolution. *Nat. Energy* **2019**, *4* (6), 512−518.
(37) Kim, Y. H.; Jeong, H.; Won, B.-R.; Jeon, H.; Park, C.-h.; Park, D.; Kim, Y.; Lee, S.; Myung, J.-h. Nanoparticle exsolution on perovskite oxides: insights into mechanism, characteristics and novel strategies. *Nano-Micro Lett.* **2024**, *16* (1), 33.
(38) Mehrer, H. History and Bibliography of Diffusion. In *Diffusion in Solids. Springer Series in Solid-State Sciences*; Springer, Berlin, Heidelberg, 2007; Vol. *155*, pp 1−18 DOI: 10.1007/978-3-540-71488-0_1.
(39) Zhang, C.; Wang, Z.; Liu, C.; Bai, Y.; Liang, C.; Low, J.; Xiong, Y. Rapid synthesis of subnanoscale high-entropy alloys with ultrahigh durability. *Nat. Mater.* **2026**, *25*, 1−9.
(40) Tao, F.; Salmeron, M. Surface restructuring and predictive design of heterogeneous catalysts. *Science* **2024**, *386* (6724), DOI: 10.1126/science.adq0102.
(41) Chi, M.; Wang, C.; Lei, Y.; Wang, G.; Li, D.; More, K. L.; Lupini, A.; Allard, L. F.; Markovic, N. M.; Stamenkovic, V. R. Surface faceting and elemental diffusion behaviour at atomic scale for alloy nanoparticles during in situ annealing. *Nat. Commun.* **2015**, *6* (1), 8925.
(42) Koo, W.-T.; Woo, S.; Shin, E.; Lee, J.; Lee, H.; Ku, K. H.; Kim, S.-J.; Kim, I.-D. Nanoscopic catalyst-loaded porous metal oxide hollow frameworks using porous block copolymer templates for high performance formaldehyde sensors. *Sens. Actuators B: Chem.* **2024**, *418*, No. 136282.
(43) Ryu, A.; Park, B.-I.; Lee, H.-J.; An, J.-W.; Kim, J.-J.; Nahm, S.; Kim, S. H.; Lee, B.; Choi, J.-W.; Jang, J.-S. Ultrafast formation of porosity and heterogeneous structures on 2D oxides via momentary photothermal effect. *J. Mater. Chem. A* **2024**, *13* (1), 561−572.
(44) Choi, S.-J.; Jang, J.-S.; Park, H. J.; Kim, I.-D. Optically sintered 2D RuO_2 nanosheets: temperature-controlled NO_2 reaction. *Adv. Funct. Mater.* **2017**, *27* (13), 1606026.
(45) Jian, G.; Zhou, L.; Piekiel, N. W.; Zachariah, M. R. Low Effective Activation Energies for Oxygen Release from Metal Oxides: Evidence for Mass-Transfer Limits at High Heating Rates. *ChemPhysChem* **2014**, *15* (8), 1666−1672.
(46) D'Angelo, A. M.; Chaffee, A. L. Correlations between oxygen uptake and vacancy concentration in Pr-doped CeO_2. *ACS Omega* **2017**, *2* (6), 2544−2551.
(47) Jeon, D.; Park, H.; Baek, J. W.; Yoon, K. R.; Kim, S.-J.; Kim, I.-D. Ultrafast photothermal shock for crystallization of vanadium oxide and in situ anchoring of Co single atoms for enhanced oxygen evolution reaction. *Chem. Commun.* **2026**, *62*, 4358−4362.
(48) Gao, M.; Zhu, L.; Peh, C. K.; Ho, G. W. Solar absorber material and system designs for photothermal water vaporization towards clean water and energy production. *Energy Environ. Sci.* **2019**, *12*, 841−864.
(49) Choi, S.-J.; Kim, S.-J; Kim, I.-D. Ultrafast optical reduction of graphene oxide sheets on colorless polyimide film for wearable chemical sensors. *NPG Asia Materials* **2016**, *8*, No. e315.
(50) Yang, S.-B.; Choi, H. K.; Lee, D. S.; Choi, C. G.; Choi, S.-Y.; Kim, I.-D. Improved optical sintering efficiency at the contacts of silver nanowires encapsulated by a graphene layer. *Small* **2015**, *11* (11), 1293−1300.

https://doi.org/10.1021/accountsmr.6c00058
Acc. Mater. Res. XXXX, XXX, XXX−XXX